Evaluating and Improving the Impact of the Atmospheric Stability and Orography on Surface Winds in the WRF Model

RAQUEL LORENTE-PLAZAS

Department of Civil and Environmental Engineering and Earth Science, University of Notre Dame, Notre Dame, Indiana, and Research Application Laboratory, National Center for Atmospheric Research, Boulder, Colorado

PEDRO A. JIMÉNEZ

Research Application Laboratory, National Center for Atmospheric Research, Boulder, Colorado

JIMY DUDHIA

Mesoscale and Microscale Meteorology Laboratory, National Center for Atmospheric Research, Boulder, Colorado

JUAN P. MONTÁVEZ

Department of Physics, University of Murcia, Murcia, Spain

(Manuscript received 29 December 2015, in final form 19 April 2016)

ABSTRACT

This study assesses the impact of the atmospheric stability on the turbulent orographic form drag (TOFD) generated by unresolved small-scale orography (SSO) focusing on surface winds. With this aim, several experiments are conducted with the Weather Research and Forecasting (WRF) Model and they are evaluated over a large number of stations (318 at 2-m height) in the Iberian Peninsula with a year of data. In WRF, Jiménez and Dudhia resolved the SSO by including a factor in the momentum equation, which is a function of the orographic variability inside a grid cell. It is found that this scheme can improve the simulated surface winds, especially at night, but it can underestimate the winds during daytime. This suggests that TOFD can be dependent on the PBL's stability. To inspect and overcome this limitation, the stability conditions are included in the SSO parameterization to maintain the intensity of the drag during stable conditions while attenuating it during unstable conditions. The numerical experiments demonstrate that the inclusion of stability effects on the SSO drag parameterization improves the simulated surface winds at diurnal, monthly, and annual scales by reducing the systematic daytime underestimation of the original scheme. The correction is especially beneficial when both the convective velocity and the boundary layer height are used to characterize the unstable conditions.

1. Introduction

The surface wind is strongly modulated by the orographic drag (Xu and Taylor 1995; Belcher and Wood 1996; Lott and Miller 1997; Rontu 2006). The intensity of this drag not only depends on the terrain features, but also on the atmospheric stability (Stull 1988; Oke 1996; Wood 2000). The modeling community, aware of the importance of representing the orographic drag in the numerical weather prediction (NWP) and climate models, has developed several approaches. As a result of these efforts, the effects that the orography exerts at the subgrid scale have been parameterized taking into account different considerations. Rontu (2006) distinguish the subgrid orography effects among the unresolved small-scale orography (SSO) and the mesoscale orography (MSO). The MSO encompasses the blocking effects and wave drags due to mesoscale mountains (e.g., Lott and Miller 1997). The unresolved SSO accounts the orographic variability generated by the presence of variable terrain elevation (e.g., several hills) inside a horizontal area, such as the grid cell of a model (e.g., Beljaars et al. 2004). Although the SSO drag affects

Corresponding author address: Raquel Lorente-Plazas, National Center for Atmospheric Research, Research Application Laboratory, 3450 Mitchell Lane, Boulder, CO 80301.
E-mail: lorente.plazas@gmail.com

DOI: 10.1175/MWR-D-15-0449.1

smaller vertical scales than the MSO (few kilometers versus up to tens of kilometers), the intensity of SSO drag can be of the same order of magnitude as the blocking/wave drag (Belcher and Wood 1996; Sandu et al. 2016). In spite of its relevance, SSO effects have received less attention in atmospheric models. This work tries to further progress on the parameterization of the SSO effects by including the stability conditions in its definition.

The SSO drag is called *turbulent orographic form drag* (TOFD). This drag was defined by Belcher and Wood (1996) as an aerodynamic force generated by the turbulent stress when orographic heterogeneities enhance the exchange of momentum. The underrepresentation of TOFD can imply an underestimation of the total subgrid surface stress. NWP and climate models parameterize this drag using different approaches. The more common approach is to use an effective roughness length (Fiedler and Panofsky 1972) that enhances the gridcell vegetative roughness length. An alternative parameterization was proposed by Wood et al. (2001) and it is based on adding a sink term in the momentum equation. Recently, Jiménez and Dudhia (2012, hereafter JD12) parameterized the SSO effects by multiplying the friction velocity by a factor that depends on the terrain features. The three methods can improve the surface wind simulation (Milton and Wilson 1996; Rontu 2006; JD12; Jiménez and Dudhia 2013; Santos-Alamillos et al. 2013; Gómez-Navarro et al. 2015) and other variables such as precipitation (Lee et al. 2015) and surface pressure (Sandu et al. 2016). A list of how the TOFD is integrated into several NWP and climate models was provided by the Working Group on Numerical Experimentation (WGNE) drag project (Zadra et al. 2013).

Most of the SSO parameterizations were developed based on observations (e.g., Grant and Mason 1990) or numerical simulations (e.g., Wood and Mason 1993) under neutral conditions, or were intended to just correct the diurnal mean wind (JD12). However, some studies have demonstrated the dependence of the TOFD with the PBL's stability. Belcher and Wood (1996) and Brown and Wood (2003) analyzed impact of the stratification on the effective roughness length. They found that weak stratification increases the wind shear in the boundary layer, which increases the TOFD. To account for this process, Belcher and Wood (1996) parameterized the roughness length as function of stratification if the height of the roughness element is smaller than the Obukhov length. Accordingly, the dependence of TOFD with the stability was one of the motivations of Wood et al. (2001) to represent the form drag using an explicit orographic-stress profile instead of the effective roughness length. This parameterization allows one to implement the effects of the stability in a more straightforward and transparent manner. The authors mentioned (but did not show) that preliminary results based on the Froude number and the Richardson number were promising. Subsequently, Allen and Brown (2006) analyzed the TOFD in convective conditions concluding that for small hills the TOFD decreases when the boundary layer becomes more convective.

In addition, Wood et al. (2001), Belcher and Wood (1996), and also Xu and Taylor (1995) suggested that the turbulence closure in modeling studies is also critical because the intensity of the orographic drag is related to the turbulence. They argued that low-order closure models produce relatively larger orographic drag because they overestimate the shear stress. On the other hand, several works (Belcher and Wood 1996; Wood et al. 2001; Sandu et al. 2016) pointed out that the inclusion of the stability on TOFD could be important when comparing it with other subgrid drags. The TOFD can be larger than surface drag or than the wave drag in stably stratified and neutral conditions, respectively.

A related issue is the use of the convective velocity to enhance the friction velocity (Beljaars 1995). When using this approach it was found (Liu et al. 2004) that the enhanced friction velocity led to an underestimation of the daytime wind, at least within the Weather Research and Forecasting (WRF) Model and the MM5 Model, the Medium-Range Forecast (MRF; Hong and Pan 1996) and Yonsei University (YSU; Hong et al. 2006 hereafter HND06) PBL schemes in those models have since removed the convective velocity contribution for surface stress while retaining it only to enhance heat and moisture fluxes. More recently, JD12 enhanced the friction velocity with a TOFD effect, but, as with the Beljaars et al. (2004) approach, stability effects were not explicitly considered. To the authors' knowledge, NWP and climate models still do not account for stability effects in the TOFD parameterizations.

This work aims to evaluate and include the effects of atmospheric stability when using the SSO drag formulation and assess its impact on the surface wind simulation. The stability effects are added to the JD12 parameterization implemented in the WRF Model (Skamarock et al. 2008). The model experiments are compared with observational data presented in Lorente-Plazas et al. (2015).

2. Model configuration and observations

The effects of the stability conditions on the SSO drag have been evaluated over the Iberian Peninsula (IP). This region was selected because both its complex

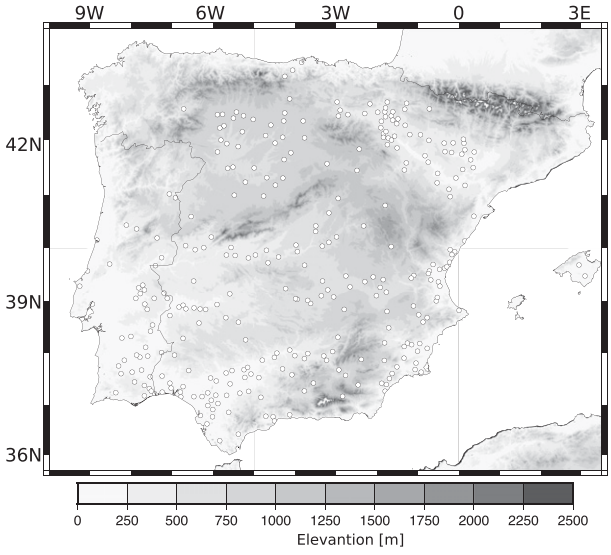

FIG. 1. The complex topography of the Iberian Peninsula is represented in gray shadow. The white circles represent the locations with wind speed observations.

orography and its location with respect to the storm track promote a wide variety of wind regimes. In addition, a dense and quality controlled database of surface wind is available for this region (Lorente-Plazas et al. 2015). For this study, 318 stations at 2 m above the ground level were selected encompassing the year of 2005 because high-quality observational data were available (Fig. 1). Similar results were obtained with a lower density of stations at 10 m (not shown).

To analyze the SSO effects several numerical experiments were performed with the WRF Model, version 3.4. The spatial configuration consists of two two-way nested domains with spatial resolutions of 10 km in the inner domain, which covers the whole IP, and 30 km in the outer domain. Vertically, 27 inhomogeneous eta levels were considered with the top level at 50 hPa and the first eta level is at 16 m approximately. The initial and boundary conditions were obtained from the ERA-Interim reanalysis (Dee et al. 2011).

Physical parameterizations are summarized in Table 1. Unresolved SSO effects are parameterized as is described in JD12 inside the PBL scheme of YSU (HND06). This scheme multiplies by a factor c_t the surface drag τ_S associated with the surface land roughness in the momentum equation; c_t is function of the standard deviation of the subgrid-scale orography and the Laplacian of the resolved orography.

Simulations are compared against the observations using the nearest grid point and removing the equivalent missing data. The wind at 2 m is diagnosed in an analogous way to 10 m using the Monin–Obukhov similarity theory consistent with the model's stability-dependent surface-layer treatment [see Jiménez et al. (2012) for details].

3. Neglecting the atmospheric stability in the SSO drag

To show the necessity of including the atmospheric conditions on SSO drag we examine the performance of the JD12 parameterization. A simulation with the SSO scheme activated (TOPO simulation) and a reference simulation without considering this scheme (REF simulation) are compared against the surface wind observations.

Figure 2 shows the annual cycle of the wind speed bias. The REF simulation overestimates the wind speed throughout the year, especially from July to December. Meanwhile TOPO simulation reduces the bias in most months, but the wind speed is underestimated, especially in the windiest months (from February to April). To gain insight into the stability dependence of this bias, the diurnal cycle of the wind speed is assessed for March (Fig. 3). This month was selected because it represents a period with a systematic underestimation of winds at night for the REF simulation during a variety of high wind speed events. The diurnal cycle shows that the TOPO simulation significantly improves the bias during the night. The TOFD acts to slow down the wind speed, which reduces the overestimation of REF simulation.

TABLE 1. Physical schemes used in the model configuration.

Parameterization	Name	Reference
Longwave radiation	Rapid Radiative Transfer Model	Mlawer et al. (1997)
Shortwave radiation	Dudhia	Dudhia (1989)
Land surface	Noah scheme	Chen and Dudhia (2001)
Cumulus	Kain–Fritsch	Kain and Fritsch (1990, 1993)
Microphysics	Single-moment 6-class (WSM6)	Hong and Lim (2006)
Surface layer	MM5 similarity (original version)	Jiménez et al. (2012)[a]
Boundary layer (PBL)	Yonsei University (YSU)	HND06

[a] The surface layer is modified to obtain the wind speed at 2 m.

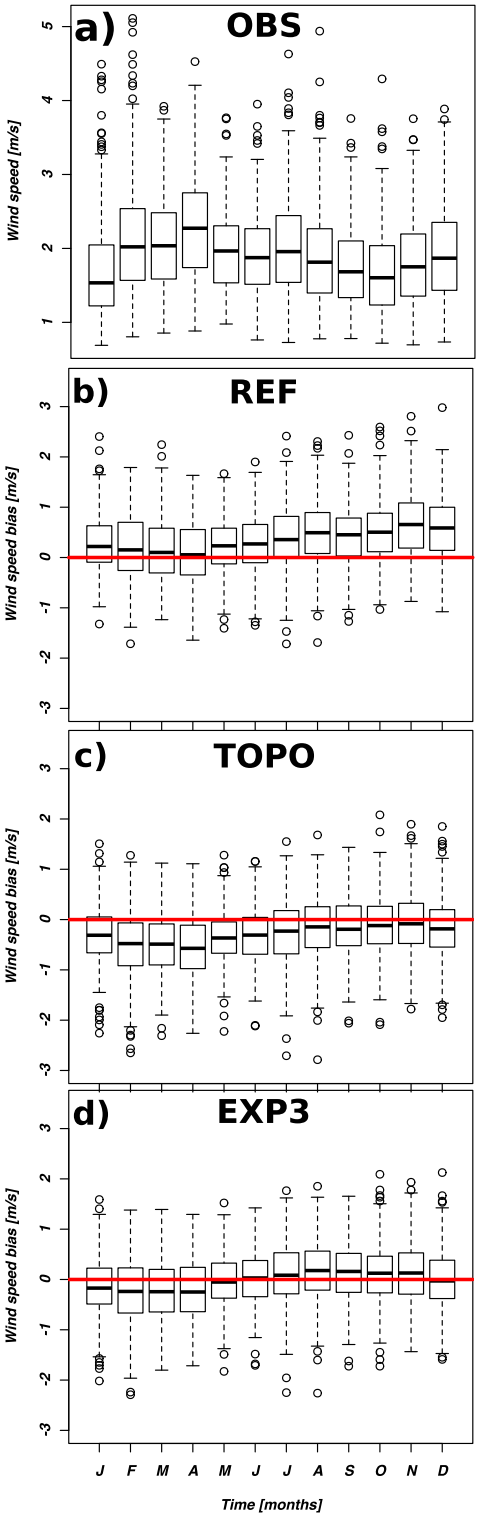

FIG. 2. Annual cycle for (a) observed wind speed, and wind speed bias for (b) REF, (c) TOPO, and (d) EXP3 simulations. Each boxplot summarized the information for all the weather stations at 2 m during 2005. The red line highlights the zero bias. Circles represent the outliers values outside the range of the probability of the whiskers. Whiskers are a 1.5 range from the first and third quartile.

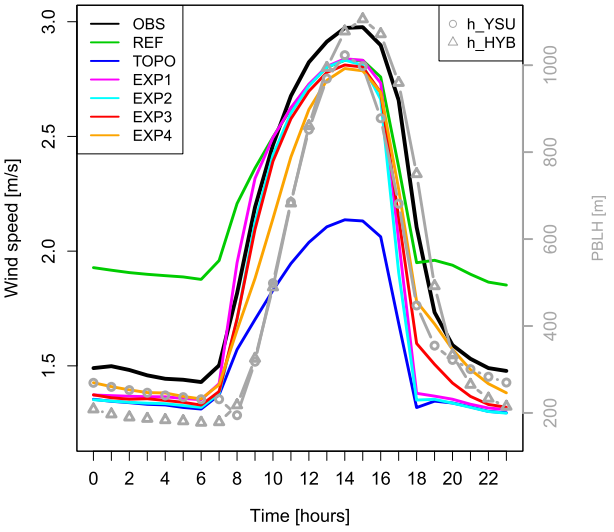

FIG. 3. Mean diurnal cycle of wind speeds for the observations (black line) and experiments (color lines). Gray lines represent the PBL height computed as YSU scheme (dots) and with the hybrid diagnosed equation (triangles). The diurnal cycle is the mean of the selected stations at 2 m for March.

Conversely, during the daytime the REF simulation captures the wind speed better than the TOPO simulation because the SSO effects overly slow down the wind speed during these more unstable conditions.

The analysis of the diurnal cycle reveals an overestimation of the TOFD during the daytime when unstable conditions dominate and suggests that the TOFD should be parameterized taking into account the PBL's activity. During the night, the stability increases, the flow near the surface is more laminar having more difficulty surmounting the SSO. Then the TOFD increases and wind speeds are decelerated. During daytime, the unstable near-surface conditions allow the flow to easily surmount the surface roughness elements, limiting the TOFD. Then the drag decreases and wind speeds are less decelerated. This points to the need to reduce the effects of form drag when the air motion is less stratified and more dominated by thermals, and the next section introduces some methods to achieve this.

4. Including the atmospheric stability in the SSO drag

a. Redefinition of the SSO drag

According to the previous results, the SSO drag must be attenuated when the flow instability increases, but it must be effective when flow stability increases. In this work, we propose a correction of the TOFD by including a term ξ that characterizes the atmospheric stability. Here ξ modulates the influence of SSO effects

by eliminating c_t during unstable conditions and including c_t during stable conditions. Then, the frictional term is redefined by

$$F = \tau_S[\xi + c_t(1-\xi)]. \quad (1)$$

If unstable conditions dominate, ξ is close to unity and only the orography-independent surface drag impacts the surface winds (as in REF; $F = \tau_S$). If stable conditions prevail, ξ is zero and the SSO drag factor multiplies surface drag (as in TOPO; $F = c_t\tau_S$); ξ will range between 0 and 1 for intermediate situations. To illustrate the impact of the atmospheric conditions on the SSO drag, four experiments (EXP1–4) have been selected which differ in the definition of the stability factor ξ.

EXP1 uses the bulk Richardson number $R_{\rm ib}$ to modulate the friction. If $R_{\rm ib} < 0$ the PBL is unstable and the SSO scheme is not included ($\xi = 1$), elsewhere the SSO is activated ($\xi = 0$). The bulk Richardson number $R_{\rm ib}$ indicates when the flow becomes turbulent and it is represented as the ratio of buoyancy to wind shear terms by

$$R_{\rm ib}(z) = \frac{g[\theta_v(z) - \theta_s]z}{\theta_{va}U(z)^2}, \quad (2)$$

where $U(z)$ is the wind speed at z vertical level, θ_s is surface virtual potential temperature, while θ_{va} and $\theta_v(z)$ are the virtual potential temperature at the lowest model level and at z vertical level, respectively. In the YSU scheme, the critical value of $R_{\rm ib}$ is 0, instead of the more common 0.25, because HND06 added an explicit entrainment layer above the PBL layer.

In EXP2, ξ is a function of the convective velocity $V_{\rm CONV}$ such that SSO is neglected when convective processes increase ($\xi = 1$) and SSO is enhanced when the convection decreases ($\xi = 0$). The convective velocity $V_{\rm CONV}$ represents the eddy wind perturbations in the near-surface layer. According to the MM5 similarity scheme in WRF, $V_{\rm CONV}$ over land is defined following Beljaars (1995) as

$$V_{\rm CONV} = \left[\frac{g}{T_s}h\left(c_p\overline{w'\theta'_v} + \frac{R_v}{R_d - 1}T_s\overline{w'q'}\right)\right]^{1/3}, \quad (3)$$

where c_p is the heat capacity at constant pressure for dry air; R_d and R_v the gas constant for dry air and water vapor, respectively; T_s the surface temperature; g/T_s the buoyancy parameter; h the boundary layer height; and $\overline{w'\theta'_v}$ and $\overline{w'q'}$ the upward flux at the surface for virtual potential temperature and moisture, respectively.

EXP3 includes a hybrid PBL height $h_{\rm HYB}$ in addition to $V_{\rm CONV}$ to reduce the c_t influence when $V_{\rm CONV}$ is zero, but the flow is still turbulent ($\xi = 1$). This hybrid PBL height is the weighted sum of the PBL height from the potential virtual temperature θ_v under unstable conditions (h_θ; Nielsen-Gammon et al. 2008) and from the TKE under stable conditions ($h_{\rm TKE}$; Banta et al. 2003), as follows:

$$h_{\rm HYB} = h_\theta W + (1 - W)h_{\rm TKE}, \quad (4)$$

where $W = 0.5\tanh[(h_\theta - h_{\rm stable})/2h_{\rm stable}] + 0.5$ and $h_{\rm stable}$ (=200 m) is a typical height of a strong nocturnal inversion. The advantage of this $h_{\rm HYB}$ instead of the θ-based one of HND06 is a better behavior under nocturnal conditions without strong surface-based forcing (Fitch et al. 2013; Benjamin et al. 2016).

The TKE is computed in the first-order YSU scheme of the PBL (HND06) by a diagnostic equation based on the level-2 simplification of the turbulent flow model proposed by Mellor and Yamada (1974, 1982). These simplifications neglect diffusion and local and advective changes of TKE, then

$$\underbrace{\frac{q^3}{16.6L}}_{\text{Dissipation}} = \underbrace{K_M\left(\overline{u'w'}\frac{\partial\overline{u}}{\partial z} + \overline{v'w'}\frac{\partial\overline{v}}{\partial z}\right)}_{\text{Shear}} - \underbrace{K_H\overline{\theta'w'}g\frac{1}{\overline{\theta}}}_{\text{Buoyancy}}, \quad (5)$$

where q^2 is twice TKE, $\overline{\theta}$ is the mean potential temperature, $\overline{u}$ and $\overline{v}$ are the mean velocity, $K_{M/H}$ are the vertical diffusion coefficients of momentum(M)/heat(H), and L is the master length scale (Blackadar 1962). The vertical turbulent fluxes ($\overline{c'w'}$; $c = u, v, \theta$) were obtained from the YSU scheme (see HND06 for details).

Finally, EXP4 combines TKE and $h_{\rm HYB}$ in the ξ definition instead of using $V_{\rm CONV}$ and $h_{\rm HYB}$ as EXP3. This allows us to examine the influence of turbulence instead of convection in the correction. EXP4 considers twice the TKE integrated over all the vertical levels (q_I^2).

The variables that represent the PBL activity ($V_{\rm CONV}$, TKE, and $h_{\rm HYB}$) were chosen by analyzing its relationship with the wind speed bias at each hour of the diurnal cycle (not shown). First, we inspected $V_{\rm CONV}$ and we found that for values larger than the unity, the bias is reduced in REF simulation from 10 to 16 h local time, but if $V_{\rm CONV}$ is less than the unity TOPO simulation reduces the bias at night hours. This motivates Eq. (1) with a threshold of unity for ξ, and the scalar functions involved in each experiment (see Table 2) were chosen taking into account this relationship in March.

b. Performance of the new SSO drag

EXP1–4 are evaluated by comparing with observations as well as with REF and TOPO simulations.

TABLE 2. Summary of the simulations performed with different frictional terms. In EXP3 and EXP4 the function of h_{HYB} is given by $f(h_{HYB}) = \max[(h_{HYB} - 500)/1000, 0]$ and in EXP4 twice the TKE (q^2) is integrated to the N vertical levels z_i such as $q_I^2 = \sum_{i=1}^{N} q_i^2/\Delta zi$.

Simulations	Stability parameter ξ in Eq. (1)
REF	1
TOPO	0
EXP1	0 if $R_{ib} > 0$, else 1
EXP2	$\min(V_{CONV}, 1)$
EXP3	$\min[0.9V_{CONV} + 1.5f(h_{HYB}), 1]$
EXP4	$\min[0.4q_I^2 + 4f(h_{HYB}), 1]$

Figure 3 shows the mean diurnal cycle of wind speed during March 2005. EXP1 (ξ function of R_{ib}) improves the diurnal cycle by reducing the nighttime (daytime) positive (negative) bias in REF (TOPO) simulations. However, an overestimation remains during sunrise and an underestimation during the late afternoon. EXP2 (ξ function of V_{CONV}) slightly reduces the wind overestimation before noon, but the negative bias during the late afternoon remains as a consequence of a sharper decline of the modeled wind speed than the observations. This issue highlights the necessity of introducing another variable that is still significant when convective forcing vanishes.

After sunset, a transitional period dominates between the unstable and stable boundary layer. Convective surface forcing vanishes and the flow is stable near the surface, but a strong downward flux remains as a result of residual turbulence and vertical wind shear in the inversion layer. The PBL mixing is still significant although V_{CONV} is zero. Therefore, a variable that represents these features of the PBL mixing is essential to reduce the wind speed bias during the late afternoon. This need motivated the choice of the PBL height diagnostic [as defined by Eq. (4)] that represents the continued effects of turbulence during the transition period. Figure 3 compares the PBL height computed by YSU scheme (h_{YSU}) and the h_{HYB} computed using the TKE. We found that h_{HYB} has its maximum higher and decreases 1 hour later than h_{YSU}.

Bearing this in mind, the h_{HYB} is included in EXP3 and EXP4 and its impact on the TOFD correction for the diurnal mean wind is shown in Fig. 3. EXP3 includes h_{HYB} in addition to V_{CONV} for the TOFD correction. The inclusion of h_{HYB} improves the wind speed during the late afternoon (18, 19, and 20 h), but a slightly negative bias still remains. Finally, EXP4 that combines q_I^2 and h_{HYB}, improves the simulated wind in these conflicting hours, but it is overestimated during the nighttime and underestimated during the early morning. Overall, EXP1–4 experiments provide more realistic diurnal cycles than the REF or TOPO simulations, which shows the relevance of atmospheric stability on the SSO effects.

Based on its best performance, EXP3 is selected to examine the SSO correction throughout the year. The annual cycle of wind speed bias (Fig. 2) shows that the systematic error is corrected, although slightly positive and negative biases remain depending on the month. The diurnal cycle of wind speed for each month (Fig. 4) shows similar results to March. The wind speed is reduced during the night and enhanced during the day with respect to REF and TOPO simulations, producing a more realistic diurnal variability. Moreover, the correction mitigates some issues. The REF wind speed overestimation is reduced during the daytime in November and December, and the TOPO daytime wind underestimation is reduced in all months. Nevertheless, the new SSO drag still overestimates during the daytime from July to October. Some preliminary spatial analysis points to this issue being attributable to deficiencies in the representation of the large-scale pressure, not related to the topography. Also, the sharp decline of wind speed in the late afternoon still remains from January to April.

5. Discussion

The generalization of the improvement of the surface winds using the JD12 scheme and its correction could be constrained by several factors; initial conditions, horizontal and vertical resolution, reforecast or continuous runs, physical parameterizations, etc. The proposed correction (as for other parameterizations) has physical fundamentals but it is also empirical. The values involved in the scalar function (Table 2) are based on the available observations with a good density of stations distributed over a heterogeneous area (with valleys, hills, coastlines, plateaus, etc.) and during a long period (1 year). This can give reliability to the parameterization. Nevertheless, sensitivity experiments are always necessary and, with further tuning, they could give more robustness to JD12 scheme and its correction for other specific practical uses.

Regarding the PBL scheme, we are using version 3.4 of the WRF Model, which is affected by an overmixing during the night due to an inappropriate representation of the nondimensional profile function in the YSU scheme during stable conditions (Hu et al. 2013). We examined this issue and we found that fixing the overmixing error enhances the SSO improvement at night by reducing the remaining bias, but it is independent of the changes we make to the daytime scheme, so those improvements remain as effective.

Regarding the technique, JD12's scheme and this correction have been included in YSU scheme, but they

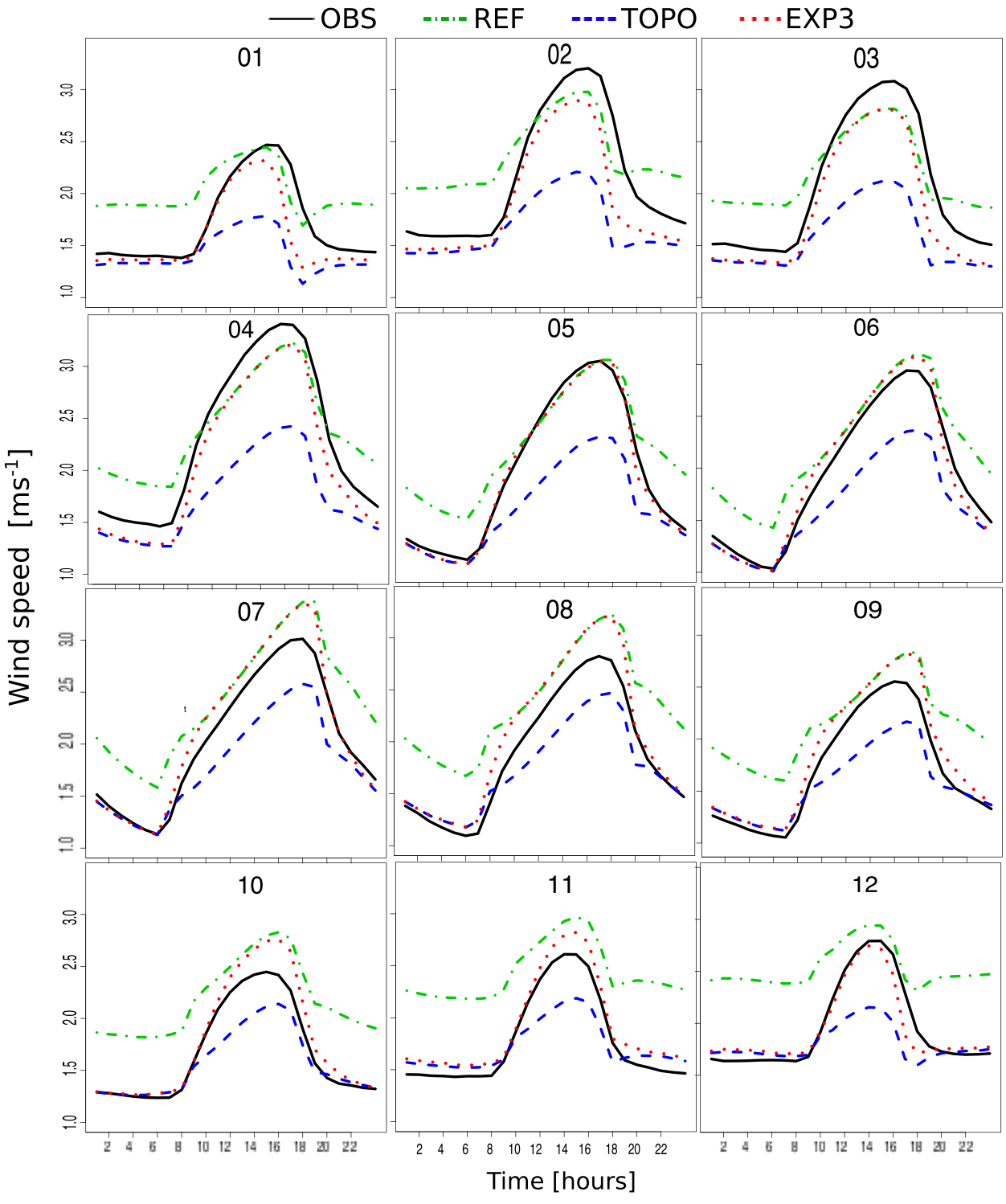

FIG. 4. Mean diurnal cycle of the wind speed for the observations (black line), REF (green line), TOPO (blue line), and EXP3 (red line) simulations. The diurnal cycle is the mean of the selected stations for each month of 2005.

can be extended to other PBL schemes. A priori, there is not any restriction because the SSO drag is based on introducing a term in the surface stress of the momentum equation so it is not dependent on the PBL scheme. Moreover, PBL schemes with an order larger than first order often compute the TKE to obtain the eddy diffusivity meaning the correction of the SSO drag could be more straightforward because then it is not necessary to diagnose the TKE as it was in our first-order scheme. On the other hand, neglect of the TOFD could be also a potential reason why other PBL schemes in the WRF Model also overestimate the winds (Shin and Hong 2011; Hu et al. 2013; Gómez-Navarro et al. 2015). Improvements in orographic drag and PBL schemes should be done together in order to avoid wrong attribution of error sources. As Sandu et al. (2016) pointed out the parameterizations of subgrid surface stress represented by the boundary layer and the subgrid orography are a major source of uncertainty in NWP and climate models.

6. Conclusions

This study assessed the role of the atmospheric stability on the drag due to unresolved small-scale orography focusing on its impact on the surface wind speed. The stability conditions are included on top of JD12's scheme that represents the SSO effects in the WRF Model using an enhanced surface stress. The necessity of including the stability effects was motivated by some limitations of the TOFD in reproducing the mean diurnal cycle of the wind speed. This scheme improved the wind speed representation during the night, but it was underestimated during the daytime. To overcome this issue, the TOFD is corrected to modulate its intensity according to the atmospheric stability. Results demonstrated how the correction maintains the intensity of the TOFD during stable conditions and decreases its intensity during unstable conditions. This correction accelerates the wind speed during the daytime, which significantly reduces the underestimation due to the JD12 method alone. Consequently, the diurnal cycle improves for all months and systematic errors in the annual cycle are removed. The benefits are especially significant when the stability is included using the convective velocity V_{CONV} and the PBL height; V_{CONV} decreases the drag when the convective processes increase. Meanwhile the PBL height reduces the drag during the late afternoon when V_{CONV} is zero and the flow still has convectively generated turbulence.

A general remark from this study is that any parameterization that attempts to include a turbulent orographic form drag should also consider the effect of stability on this extra drag, and, in particular, that under convective boundary layer conditions, this form drag may reduce significantly in magnitude.

Acknowledgments. This study was partially supported by the Fondo Europeo de Desarrollo Regional (FEDER) through the SPEQ-TRES Project (CGL2011-29672-C02-02), REPAIR (CGL2014-59677-R), and by the Mountain Terrain Atmospheric Modeling and Observation Program (MATERHORN). J.P. Montávez also acknowledges financial support from Fundación Seneca (Ref. 19640/EE/14). The first three authors acknowledge the support of NCAR facilities by the National Science Foundation. The authors also thank Hyeyum Hailey Shin for her early discussions about the TKE computation. We also acknowledge three anonymous reviewers and Daniel Kirshbaum whose comments improved the manuscript.

REFERENCES

Allen, T., and A. R. Brown, 2006: Modelling of turbulent form drag in convective conditions. *Bound.-Layer Meteor.*, **118**, 421–429, doi:10.1007/s10546-005-9002-z.

Banta, R. M., Y. L. Pichugina, and R. K. Newsom, 2003: Relationship between low-level jet properties and turbulence kinetic energy in the nocturnal stable boundary layer. *J. Atmos. Sci.*, **60**, 2549–2555, doi:10.1175/1520-0469(2003)060<2549:RBLJPA>2.0.CO;2.

Belcher, S., and N. Wood, 1996: Form and wave drag due to stably stratified turbulent flow over low ridges. *Quart. J. Roy. Meteor. Soc.*, **122**, 863–902, doi:10.1002/qj.49712253205.

Beljaars, A. C. M., 1995: The parameterization of surface fluxes in large-scale models under free convection. *Quart. J. Roy. Meteor. Soc.*, **121**, 255–270, doi:10.1002/qj.49712152203.

——, A. R. Brown, and N. Wood, 2004: A new parametrization of turbulent orographic form drag. *Quart. J. Roy. Meteor. Soc.*, **130**, 1327–1347, doi:10.1256/qj.03.73.

Benjamin, S. G., and Coauthors, 2016: A North American hourly assimilation and model forecast cycle: The rapid refresh. *Mon. Wea. Rev.*, **144**, 1669–1694, doi:10.1175/MWR-D-15-0242.1.

Blackadar, A. K., 1962: The vertical distribution of wind and turbulent exchange in a neutral atmosphere. *J. Geophys. Res.*, **67**, 3095–3102, doi:10.1029/JZ067i008p03095.

Brown, A. R., and N. Wood, 2003: Properties and parameterization of the stable boundary layer over moderate topography. *J. Atmos. Sci.*, **60**, 2797–2808, doi:10.1175/1520-0469(2003)060<2797:PAPOTS>2.0.CO;2.

Chen, F., and J. Dudhia, 2001: Coupling an advanced land surface-hydrology model with the Penn State/NCAR MM5 Modeling System. Part I: Model description and implementation. *Mon. Wea. Rev.*, **129**, 569–586, doi:10.1175/1520-0493(2001)129<0569:CAALSH>2.0.CO;2.

Dee, D. P., and Coauthors, 2011: The ERA-Interim reanalysis: Configuration and performance of the data assimilation system. *Quart. J. Roy. Meteor. Soc.*, **137**, 553–597, doi:10.1002/qj.828.

Dudhia, J., 1989: Numerical study of convection observed during the winter monsoon experiment using a mesoscale two-dimensional model. *J. Atmos. Sci.*, **46**, 3077–3107, doi:10.1175/1520-0469(1989)046<3077:NSOCOD>2.0.CO;2.

Fiedler, F., and H. A. Panofsky, 1972: The geostrophic drag coefficient and the 'effective' roughness length. *Quart. J. Roy. Meteor. Soc.*, **98**, 213–220, doi:10.1002/qj.49709841519.

Fitch, A. C., J. K. Lundquist, and J. B. Olson, 2013: Mesoscale influences of wind farms throughout a diurnal cycle. *Mon. Wea. Rev.*, **141**, 2173–2198, doi:10.1175/MWR-D-12-00185.1.

Gómez-Navarro, J. J., C. C. Raible, and S. Dierer, 2015: Sensitivity of the WRF model to PBL parametrizations and nesting techniques: Evaluation of surface wind over complex terrain. *Geosci. Model Dev. Discuss.*, **8**, 5437–5479, doi:10.5194/gmdd-8-5437-2015.

Grant, A. L. M., and P. J. Mason, 1990: Observations of boundary-layer structure over complex terrain. *Quart. J. Roy. Meteor. Soc.*, **116**, 159–186, doi:10.1002/qj.49711649107.

Hong, S.-Y., and H. L. Pan, 1996: Nonlocal boundary layer vertical diffusion in a medium-range forecast model. *Mon. Wea. Rev.*, **124**, 2322–2339, doi:10.1175/1520-0493(1996)124<2322:NBLVDI>2.0.CO;2.

——, and J.-O. Lim, 2006: The WRF single-moment 6-class microphysics scheme (WSM6). *J. Korean Meteor. Soc.*, **42** (2), 129–151.

——, Y. Noh, and J. Dudhia, 2006: A new vertical diffusion package with an explicit treatment of entrainment processes. *Mon. Wea. Rev.*, **134**, 2318–2341, doi:10.1175/MWR3199.1.

Hu, X.-M., P. M. Klein, and M. Xue, 2013: Evaluation of the updated YSU planetary boundary layer scheme within WRF for wind resource and air quality assessments. *J. Geophys. Res. Atmos.*, **118**, 10 490–10 505, doi:10.1002/jgrd.50823.

Jiménez, P. A., and J. Dudhia, 2012: Improving the representation of resolved and unresolved topographic effects on surface wind in the WRF model. *J. Appl. Meteor. Climatol.*, **51**, 300–316, doi:10.1175/JAMC-D-11-084.1.

——, and ——, 2013: On the ability of the WRF model to reproduce the surface wind direction over complex terrain. *J. Appl. Meteor. Climatol.*, **52**, 1610–1617, doi:10.1175/JAMC-D-12-0266.1.

——, ——, J. F. González-Rouco, J. Navarro, J. P. Montávez, and E. García-Bustamante, 2012: A revised scheme for the WRF surface layer formulation. *Mon. Wea. Rev.*, **140**, 898–918, doi:10.1175/MWR-D-11-00056.1.

Kain, J. S., and J. M. Fritsch, 1990: A one-dimensional entraining/detraining plume model and its application in convective parameterization. *J. Atmos. Sci.*, **47**, 2784–2802, doi:10.1175/1520-0469(1990)047<2784:AODEPM>2.0.CO;2.

——, and ——, 1993: Convective parameterization for mesoscale models: The Kain-Fritsch scheme. The *Representation* of *Cumulus Convection* in *Numerical Models, Meteor. Monogr.*, No. 46, Amer. Meteor. Soc., 165–170.

Lee, J., H. H. Shin, S.-Y. Hong, P. A. Jiménez, J. Dudhia, and J. Hong, 2015: Impacts of subgrid-scale orography parameterization on simulated surface layer wind and monsoonal precipitation in the high-resolution WRF model. *J. Geophys. Res. Atmos.*, **120**, 644–653, doi:10.1002/2014JD022747.

Liu, Y., F. Chen, T. Warner, S. Swerdlin, J. Bowers, and S. Halvorson, 2004: Improvements to surface flux computations in a non-local-mixing PBL scheme, and refinements on urban processes in the NOAH land-surface model with the NCAR/ATEC real-time FDDA and forecast system. *20th Conf. on Weather Analysis and Forecasting/16th Conf. on Numerical Weather Prediction*, Seattle, WA, Amer. Meteor. Soc., 22.2. [Available online at https://ams.confex.com/ams/84Annual/techprogram/paper_72489.htm.]

Lorente-Plazas, R., J. P. Montávez, P. A. Jimenez, S. Jerez, J. J. Gómez-Navarro, J. A. Garcia-Valero, and P. Jimenez-Guerrero, 2015: Characterization of surface winds over the Iberian Peninsula. *Int. J. Climatol.*, **35**, 1007–1026, doi:10.1002/joc.4034.

Lott, F., and M. Miller, 1997: A new subgrid-scale orographic drag parametrization: Its formulation and testing. *Quart. J. Roy. Meteor. Soc.*, **123**, 101–127, doi:10.1002/qj.49712353704.

Mellor, G., and T. Yamada, 1974: A hierarchy of turbulence closure models for planetary boundary layers. *J. Atmos. Sci.*, **31**, 1791–1806, doi:10.1175/1520-0469(1974)031<1791:AHOTCM>2.0.CO;2.

——, and ——, 1982: Development of a turbulence closure model for geophysical fluid problems. *Rev. Geophys.*, **20**, 851–875, doi:10.1029/RG020i004p00851.

Milton, S. F., and C. A. Wilson, 1996: The impact of parameterized subgrid-scale orographic forcing on systematic errors in a global NWP model. *Mon. Wea. Rev.*, **124**, 2023–2045, doi:10.1175/1520-0493(1996)124<2023:TIOPSS>2.0.CO;2.

Mlawer, E. J., S. J. Taubman, P. D. Brown, M. J. Iacono, and S. A. Clough, 1997: Radiative transfer for inhomogeneous atmospheres: RRTM, a validated correlated-k model for the longwave. *J. Geophys. Res.*, **102**, 16 663–16 682, doi:10.1029/97JD00237.

Nielsen-Gammon, J. W., and Coauthors, 2008: Multisensor estimation of mixing heights over a coastal city. *J. Appl. Meteor. Climatol.*, **47**, 27–43, doi:10.1175/2007JAMC1503.1.

Oke, T., 1996: *Boundary Layer Climates*. 2nd ed. University Press, 345 pp.

Rontu, L., 2006: A study on parametrization of orography-related momentum fluxes in a synoptic-scale NWP model. *Tellus*, **58A**, 69–81, doi:10.1111/j.1600-0870.2006.00162.x.

Sandu, I., P. Bechtold, A. Beljaars, A. Bozzo, F. Pithan, T. G. Shepherd, and A. Zadra, 2016: Impacts of parameterized orographic drag on the Northern Hemisphere winter circulation. *J. Adv. Model. Earth Syst.*, **8**, 196–211, doi:10.1002/2015MS000564.

Santos-Alamillos, F., D. Pozo-Vázquez, J. Ruiz-Arias, V. Lara-Fanego, and J. Tovar-Pescador, 2013: Analysis of WRF Model wind estimate sensitivity to physics parameterization choice and terrain representation in Andalusia (southern Spain). *J. Appl. Meteor. Climatol.*, **52**, 1592–1609, doi:10.1175/JAMC-D-12-0204.1.

Shin, H. H., and S.-Y. Hong, 2011: Intercomparison of planetary boundary-layer parametrizations in the WRF model for a single day from CASES-99. *Bound.-Layer Meteor.*, **139**, 261–281, doi:10.1007/s10546-010-9583-z.

Skamarock, W. C., and Coauthors, 2008: A description of the Advanced Research WRF version 3. NCAR Tech. Note NCAR/TN-475+STR, 113 pp., doi:10.5065/D68S4MVH.

Stull, R., 1988: *An Introduction to Boundary Layer Meteorology*. Kluwer Academic Publishers, 670 pp.

Wood, N., 2000: Wind flow over complex terrain: A historical perspective and the prospect for large-eddy modelling. *Bound.-Layer Meteor.*, **96**, 11–32, doi:10.1023/A:1002017732694.

——, and P. Mason, 1993: The pressure force induced by neutral, turbulent flow over hills. *Quart. J. Roy. Meteor. Soc.*, **119**, 1233–1267, doi:10.1002/qj.49711951402.

——, A. Brown, and F. Hewer, 2001: Parametrizing the effects of orography on the boundary layer: An alternative to effective roughness lengths. *Quart. J. Roy. Meteor. Soc.*, **127**, 759–777, doi:10.1002/qj.49712757303.

Xu, D., and P. A. Taylor, 1995: Boundary-layer parametrization of drag over small-scale topography. *Quart. J. Roy. Meteor. Soc.*, **121**, 433–443, doi:10.1002/qj.49712152210.

Zadra, A., and Coauthors, 2013: WGNE Drag Project—An intermodel comparison of surface stresses. Rep. 1, Atmosperic Numerical Weather Prediction Research Division, Environment Canada, 36 pp. [Available online at http://collaboration.cmc.ec.gc.ca/science/rpn/drag_project/documents/wgne_drag_project_report01.pdf.]